Infrared Photorefractive Polymers and Their Applications for Imaging

B. Kippelen,* S. R. Marder,* E. Hendrickx, J. L. Maldonado, G. Guillemet, B. L. Volodin, D. D. Steele, Y. Enami, Sandalphon, Y. J. Yao, J. F. Wang, H. Röckel, L. Erskine, N. Peyghambarian*

Photorefractive polymers with high diffraction efficiency in the visible and near-infrared regions of the electromagnetic spectrum have been developed. These polymers, which have a large dynamic range because of their high orientational birefringence, incorporate a dye designed to have a large dipole moment and a high linear polarizability anisotropy. Such polymers have enabled demonstrations of imaging through scattering media, using a holographic time-gating technique at a wavelength that is compatible with the transparency of biological tissues and with the emission of low-cost semiconductor laser diodes.

The photorefractive (PR) effect enables the recording of optical information in three-dimensional solids through the optical generation of an internal space-charge field that gives rise to refractive index changes in the material (*1, 2*). Because of their high optical sensitivity and the ability to erase and rewrite information optically in real time, materials that exhibit the PR effect are expected to play a major role in photonic technologies. For applications based on recording and retrieval of stored holograms, the important material parameter is the dynamic range (or index modulation) Δn, and one of the current challenges is to increase this Δn. PR materials with large dynamic range enable real-time holographic applications such as imaging through scattering media.

Recently, polymers have emerged as new PR materials (*3–10*). They have considerable technological potential because of their high efficiency and their ability to be easily processed into large-area films at low cost. With the rapid improvement of the performance of guest-host PR polymer composites (*8–9*) and the report of near 100% diffraction efficiency in 105-μm-thick samples (*10*), it became apparent that a linear electro-optic effect alone could not account for the origin of the large changes in the refractive index. An explanation was provided with the orientational enhancement model proposed by Moerner and co-workers (*11*), in which both the birefringence induced by the orientation of the molecules (*12, 13*) and the electro-optic properties contribute to the refractive index modulation changes. Thus, on a molecular level, according to the oriented gas model (*14, 15*), the following figure of merit may be defined for the optimization of the PR effect: $F = A(T)\Delta\alpha\mu^2 + \beta\mu$, where $\Delta\alpha$ is the polarizability anisotropy of the chromophore, μ is its dipole moment, β is its first hyperpolarizability, and $A(T) = 2/(9kT)$ is a scaling factor (kT is the thermal energy). Early dopant molecules such as 3-fluoro-4-*N*,*N*-diethylamino-β-nitrostyrene (FDEANST) and 2,5-dimethyl-4-*p*-nitrophenylazoanisole (DMNPAA) were incorporated into polymer composites because of their electro-optic properties. More recent organic PR materials (*16*) were based on molecules such as *N*-2-butyl-2,6-dimethyl-4*H*-pyridone-4-ylidenecyanomethylacetate (2BNCM) with large $\Delta\alpha$, which enabled improvement of the dynamic range by a factor of 1.5 over the best previous PR polymers doped with DMNPAA (*17*). Model calculations using the bond order alternation theory (*18*) have shown that the orientational birefringence contribution is optimized for molecules that are polarized beyond the cyanine limit, that is, for molecules with high values of both μ and $\Delta\alpha$.

To explore this design rationale, we have focused our studies on linear molecules such as polyenes, rather than on chromophores that contain benzene rings. This is because the former exhibit a considerable charge transfer that is confined along the quasi one-dimensional π-conjugated bridge, providing a large $\Delta\alpha$. In addition, polyenes can have an important charge separation in the ground state that provides a large μ. To comply with the practical requirements of a well-performing PR polymer, we synthesized the polyene molecule 2-*N*,*N*-dihexylamino-7-dicyanomethylidenyl-3,4,5,6,10-pentahydronaphthalene (DHADC-MPN) (Fig. 1). The hexyl groups help impart solubility to this highly dipolar molecule. The incorporation of the polyene into the fused-ring systems enhances thermal and

Table 1. Numbering scheme and PR properties of several polymer composites (*n*, average refractive index; Δn, index modulation at 40 V μm^{-1}).

Sample and composition (weight %)	λ (nm)	*n*	$E_{\pi/2}$ (V μm^{-1})	η_{max} (%)	Δn
1 DHADC-MPN:PVK:ECZ:TNF (40:39:19:2)	633	1.77	30	10	0.0044
2 DMNPAA:PVK:ECZ:TNF (40:39:19:2)	633	1.75	65	54	0.0009
3 NPADVBB:PVK:ECZ:TNF (40:39:19:2)	633	1.71	65	51	0.0009
4 DHADC-MPN:PVK:ECZ:TNFDM (25:49:24:2)	830	1.69	59	30	0.0015
5 DHADC-MPN:PVK:ECZ:TNFDM (25:49:25:1)	830	1.69	59	74	0.0015
6 NPADVBB:PVK:ECZ:TNFDM (40:39:19:2)	830	1.69	–	15*	0.00025
7 DMNPAA:PVK:ECZ:TNF (50:33:16:1)	675	1.75	60	86	0.0012
2BNCM:PMMA:TNF (90:10:0.3)	676	–	48†	80	0.0019

*At 85 V μm^{-1}. †Extrapolated from (*16*) for a 105-μm-thick sample (*17*).

B. Kippelen, E. Hendrickx, J. L. Maldonado, G. Guillemet, B. L. Volodin, D. D. Steele, Y. Enami, Sandalphon, Y. J. Yao, J. F. Wang, N. Peyghambarian, Optical Sciences Center, University of Arizona, Tucson, AZ 85721, USA.
S. R. Marder, Beckman Institute, California Institute of Technology, Pasadena, CA 91125, USA, and Jet Propulsion Laboratory, California Institute of Technology, Pasadena, CA 91109, USA.
H. Röckel and L. Erskine, Beckman Institute, California Institute of Technology, Pasadena, CA 91125, USA.

*To whom correspondence should be addressed. E-mail: kippelen@u.arizona.edu, srm@cco.caltech.edu, and nnp@u.arizona.edu

photochemical stability. The molecule was used as a dopant molecule in mixtures of poly(*N*-vinylcarbazole) (PVK) and *N*-ethylcarbazole (ECZ). Sensitivity in the visible (633 nm) was provided by 2,4,7-trinitrofluorenone (TNF). By using the sensitizer (2,4,7-trinitro-9-fluorenylidene)malonitrile (TNFDM), the spectral response of the photosensitivity could be extended to the near-IR (830 nm).

The PR properties, in particular the dynamic range Δn, were tested by four-wave mixing experiments in a tilted geometry (Fig. 2A). The thickness of all the samples was 105 μm and the polymer was sandwiched between two transparent indium–tin oxide (ITO) electrodes. Under these conditions, the gratings written in the composites can be considered as thick, and their diffraction efficiency η can be modeled using Kogelnik's coupled-wave theory (*19*). Two-beam coupling—that is, energy exchange between the two interfering laser beams—was observed in all the PR composites presented here and confirmed the PR nature of the optical encoding (*1*, *5*, *7*). To evaluate the new dopant molecule, we carried out four-wave mixing experiments in various samples with different dopant molecules, including DMNPAA (*10*) and isomeric mixtures of 4-(4′-nitrophenylazo)-1,3-di[(3′′ or 4′′-vinyl)benzyloxy]-benzene (NPADVBB), and at different wavelengths λ. Data were obtained for s-polarized writing beams and a p-polarized reading beam (Table 1). For composites **1** to **6**, the diffraction efficiency as a function of applied field follows the oscillatory behavior of the $\sin^2$ functional dependence of the diffraction efficiency predicted by Kogelnik's theory (*19*). $E_{\pi/2}$ is the applied field where maximum diffraction is observed. The diffraction efficiency at this maximum (η_{max}) is mainly limited by the absorption of the sample and reflection losses. Composites **1** and **2** exhibit a first maximum of the normalized diffraction efficiency (normalized to the value measured at $E_{\pi/2}$ and corrected for small electro-absorption effects) at applied fields $E_{\pi/2}$ = 30 V μm^{-1} and $E_{\pi/2}$ = 65 V μm^{-1}, respectively (Fig. 2B). At this first maximum of the diffraction efficiency, $\nu = \pi/2$ in Kogelnik's expression for the diffraction efficiency (*19*). This reduction in $E_{\pi/2}$ by a factor larger than 2 is indicative of the better efficiency of DHADC-MPN–based polymers. Calculations of Δn using Kogelnik's expression (*19*) (Table 1) show that Δn in composite **1** is more than four times that in composite **2** at the same applied field of 40 V μm^{-1}. By replacing TNF by TNFDM as a sensitizer, the spectral sensitivity of polymer composites **4** to **6** (Table 1) was extended to the near infrared (IR). In the normalized diffraction efficiency of composite **4** at 830 nm (Fig. 3), maximum diffraction is observed at $E_{\pi/2}$ = 59 V μm^{-1}. The real diffraction efficiency η_{max} at $E_{\pi/2}$ is 30% for composite **4** (Table 1). This value can be further optimized by reducing the sensitizer concentration, that is, reducing the absorption of the sample at 830 nm, as illustrated by η_{max} = 74% in composite **5** (Table 1).

To demonstrate the practical use of these new materials, we performed aging tests at elevated temperature to characterize their phase stability. Accelerated aging studies at 85°C using the optical scattering setup described in (*20*) indicate that NPADVBB-based and DHADC-MPN–based samples have a lifetime of several years at room temperature. As shown in Fig. 3B for composite **5**, the samples exhibit a recording speed of a few seconds.

To get further structure-property relations between the dopant molecules and the PR performance of the composite, we performed independent frequency-dependent ellipsometry (FDE) experiments. Following the procedure described in (*21*), the quantities $\Delta\alpha\mu^2$ and $\beta\mu$ can be evaluated

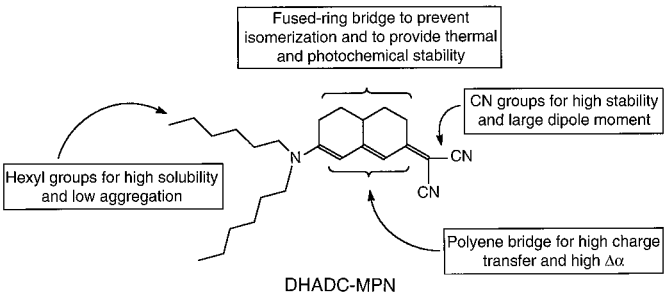

Fig. 1. Chemical structure and design strategy of the DHADC-MPN molecule. The identification of the compound was determined by nuclear magnetic resonance, ultraviolet-visible and mass spectroscopy, and elemental analysis (*27*).

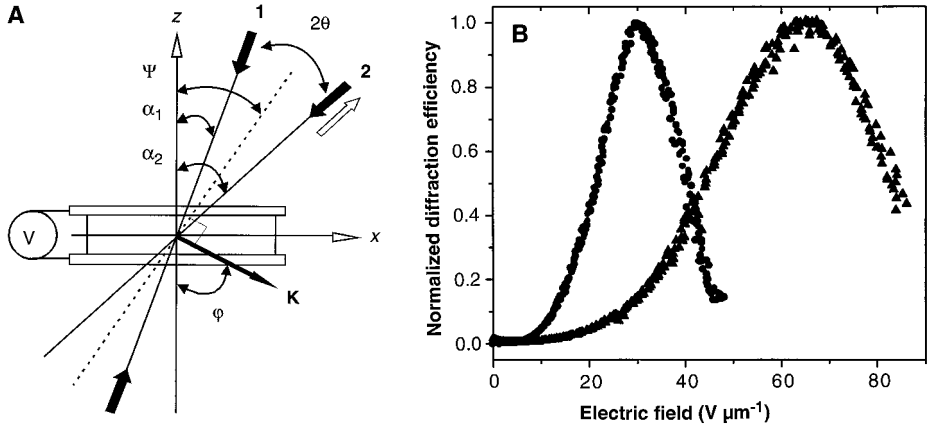

Fig. 2. (**A**) Tilted four-wave mixing geometry. **K** is the grating vector, ψ = 60°, and 2θ = 20°. (**B**) Normalized diffraction efficiency versus field measured at 633 nm in composites **1** (circles) and **2** (triangles). For sample **1**, $I_1 = I_2$ = 0.4 W cm^{-2} and I_p = 1 mW cm^{-2}, where I_1 and I_2 are the power densities of the writing beams and I_p is the power density of the reading beam. For sample **2**, $I_1 = I_2$ = 0.7 W cm^{-2} and I_p = 0.6 mW cm^{-2}.

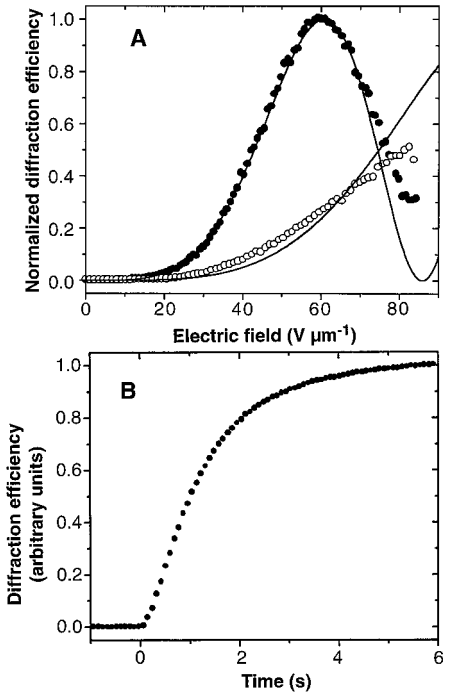

Fig. 3. (**A**) Normalized diffraction efficiency versus field measured at 830 nm in composite **4** for s-polarized writing beams, for s-polarized readout (empty circles), and for p-polarized readout (full circles). $I_1 = I_2$ = 0.28 W cm^{-2} and I_p = 1 mW cm^{-2}. The solid lines are theoretical fits. (**B**) Build-up time in sample **5** at 830 nm for an applied field of 29 V μm^{-1} and for $I_1 = I_2$ = 0.5 W cm^{-2}, I_p = 1 mW cm^{-2}.

in the solid matrix by using the oriented gas model. With independent dipole moment measurements in solution and dielectric constant measurements of the polymer films, $\Delta\alpha$ and β could be obtained for DHADC-MPN, DMNPAA, and NPAD-VBB (Table 2). The dispersion-free value of the electro-optic hyperpolarizability β_0^{EO} was calculated using the standard dispersion formula given by the two-level model for an electro-optic process (*22*) [$\beta_0^{EO} \neq \beta_0$, where β_0 is deduced from electric field–induced second harmonic generation (EFISH) experiments]. Independently, we deduced molecular parameters from the model calculations (*7, 11*) of the diffraction efficiency for s- and p-polarized readout described above (solid lines in Fig. 3A) and by assuming that the space-charge field was given by the component of the applied field along the grating vector **K** (Fig. 2A). This analysis was carried out for composites **4**, **6**, and **7** (values in parentheses in Table 2). These calculations do not have any adjustable parameters. Good agreement between the values of $\Delta\alpha$ and β_0^{EO} deduced from the two types of independent experiments is obtained. The orientational contribution $A(T)\mu^2\Delta\alpha/M$ (where M is the molecular weight) calculated for the different molecules (Table 2) shows the high orientational birefringence of DHADC-MPN. This result suggests that our proposed design rationale (*18*)—that is, to synthesize molecules that combine high μ and high $\Delta\alpha$—provides an efficient route to optimizing the performance of low–glass transition temperature PR polymers.

The PR polymer composites with large Δn and spectral sensitivity in the near IR developed here offer opportunities for numerous photonic applications. As a sensitive holographic recording medium with high Δn, they can be used for imaging through scattering media. Of particular importance is their compatibility with the emission of high-quality GaAs semiconductor laser diodes and commercial solid-state femtosecond lasers, such as Ti:sapphire lasers. More important, their near IR spectral response is compatible with the transparency of biological tissues (700 to 900 nm), and therefore the imaging technique shown here could be extended to medical imaging. Imaging with optical radiation would provide a valuable tool for diagnostics of biological tissues if the highly scattered light could be separated from the small amount of unscattered light (or ballistic light) that carries useful information about absorption centers in the medium.

Holographic time gating (HTG) (*23, 24*) is a direct imaging technique that uses the coherence properties of the ballistic light to filter out the diffuse light. In this method, a hologram is formed between the ballistic light of an object beam and a reference beam. The light can be provided either by a short-pulse laser source or by a low-coherence laser source such as a superluminescent laser diode. Filtering is then achieved by adjusting the relative time delay between the object and the reference beams. When using short pulses, a hologram of the ballistic light is formed by adjusting its temporal overlap with the reference pulse. In this case, the scattered light is delayed with respect to the ballistic light and does not overlap in time with the reference pulse to form a hologram. The information carried by the ballistic light is then reconstructed by reading out the recorded hologram in the four-wave mixing geometry (Fig. 4). When using low-coherence continuous wave (cw) lasers, the hologram is formed only when the relative path of the two beams is within the coherence length of the laser source. In this case, the delayed scattered light does not interfere with the reference beam and does not contribute to the hologram formation.

To demonstrate imaging using HTG and the newly developed IR-sensitive polymers, we used a Ti:sapphire laser in either pulsed or cw regime (*25*). Imaging was achieved at 800 nm through suspensions of calibrated polystyrene microspheres in water. Using the laser in cw low-coherence operation, we were able to reconstruct an image through a solution with an effective optical density of 4 (Fig. 4). The good optical quality that was obtained clearly demonstrates the potential of the technique. Highly efficient PR polymers offer a number of advantages over the recording media used for HTG in the past [such as photographic emulsions, charge-coupled devices, and rhodium-doped $BaTiO_3$ (*26*)]. Because of their high sensitivity and large Δn, hologram reconstruction efficiencies close to unity can be achieved in 100-μm-thick films (compared with several millimeters for inorganic crystals), providing wide angular bandwidth and consequently high image resolution. Moreover, the response time of polymers is one-tenth that of $BaTiO_3$ crystals (*26*). Relative to other imaging techniques, this method potentially offers a fast acquisition time because no scanning, computation, or digital processing is involved. Because of the use of a highly efficient PR polymer with low cost as recording material and its compatibility with superluminescent low-coherence laser diodes, the manufacturing cost of such a system would be low. Therefore, this imaging technique could become a valuable new medical diagnosis tool.

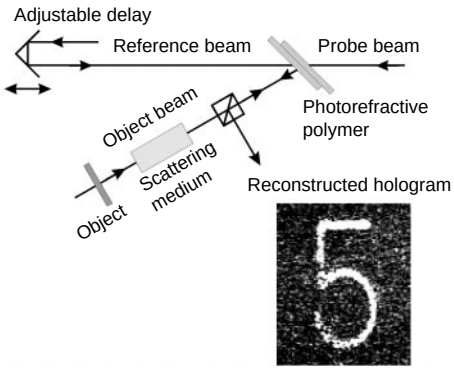

Fig. 4. Four-wave mixing configuration used for the HTG experiments. The reconstructed hologram was obtained using sample **5** with an applied voltage of 5.5 kV. The average power of the Ti:sapphire laser was 250 mW.

Table 2. Molecular constants of DHADC-MPN, DMNPAA, and NPADVBB, determined in three polymer composites (numbers defined in Table 1) from FDE experiments at several wavelengths and from four-wave mixing experiments (values in parentheses) using the oriented gas model.

Sample	Chromophore				
	λ (nm)	μ (10^{-18} esu)	$\Delta\alpha$ (10^{-23} esu)	β_0^{EO} (10^{-30} esu)	$A(T)\mu^2\Delta\alpha/M$ (10^{-48})
4	830	12	2.3 (2.7)	63 (63)	45 (55)
7	690	5.5	3.9 (4.4)	48 (65)	22 (25)
6	633	7.4	2.5 (3.9)	26 (60)	15 (23)
	830	7.4	1.7	26	10

REFERENCES AND NOTES

1. P. Günter and J.-P. Huignard, *Photorefractive Materials and Their Applications* (Springer, Berlin, 1988), vol. 1; *ibid*. (1989), vol. 2.
2. A. Ashkin *et al.*, *Appl. Phys. Lett.* **9**, 72 (1966).
3. B. Volodin, B. Kippelen, K. Meerholz, B. Javidi, N. Peyghambarian, *Nature* **383**, 58 (1996).
4. S. Ducharme, J. C. Scott, R. J. Twieg, W. E. Moerner, *Phys. Rev. Lett.* **66**, 1846 (1991).
5. W. E. Moerner and S. M. Silence, *Chem. Rev.* **94**, 127 (1994); A. Grunnet-Jepsen, C. L. Thomson, W. E. Moerner, *Science* **277**, 549 (1997).
6. Y. Zhang, R. Burzynski, S. Ghosal, M. K. Casstevens, *Adv. Mater.* **8**, 111 (1996).
7. B. Kippelen, K. Meerholz, N. Peyghambarian, in *Nonlinear Optics of Organic Molecules and Polymers,* H. S. Nalwa and S. Miyata, Eds. (CRC Press, Boca Raton, FL, 1997), pp. 465–513.
8. M. C. J. M. Donckers *et al.*, *Opt. Lett.* **18**, 1044 (1993).

9. M. Liphardt *et al.*, *Science* **263**, 367 (1994).
10. K. Meerholz, B. L. Volodin, Sandalphon, B. Kippelen, N. Peyghambarian, *Nature* **371**, 497 (1994).
11. W. E. Moerner, S. M. Silence, F. Hache, G. C. Bjorklund, *J. Opt. Soc. Am. B* **11**, 320 (1994).
12. M. G. Kuzyk, J. E. Sohn, C. W. Dirk, *ibid*. **7**, 842 (1990).
13. J. W. Wu, *ibid*. **8**, 142 (1991).
14. D. J. Williams, in *Nonlinear Optical Properties of Organic Molecules and Crystals*, D. S. Chemla and J. Zyss, Eds. (Academic Press, Orlando, FL, 1987), vol. 1.
15. K. D. Singer, M. G. Kuzyk, J. E. Sohn, *J. Opt. Soc. Am. B* **4**, 968 (1987).
16. P. M. Lundquist *et al.*, *Science* **274**, 1182 (1996).
17. The value for Δn reported in table 2 of (*16*) for a sample with composition 2BNCM:PMMA:TNF 90:10:0.3 weight % is 10×10^{-3}. However, to be consistent with the four-wave mixing results presented in figure 1 of (*16*), this value should read 1.5×10^{-3}.
18. B. Kippelen, F. Meyers, N. Peyghambarian, S. R. Marder, *J. Am. Chem. Soc.* **119**, 4559 (1997).
19. H. Kogelnik, *Bell. Syst. Tech. J.* **48**, 2909 (1969). Kogelnik's coupled-wave theory for thick phase gratings predicts that the diffraction efficiency η is given by $\eta \propto \sin^2 \nu$ with $\nu = G\pi\Delta nd/\lambda$, where G is a geometrical factor that depends on the polarization of the beams and the experimental geometry, Δn is the dynamic range, d is the thickness of the grating, and λ is the wavelength of the light.
20. E. Hendrickx *et al.*, *Appl. Phys. Lett.* **71**, 1159 (1997).
21. B. Kippelen, Sandalphon, K. Meerholz, N. Peyghambarian, *ibid.* **68**, 1748 (1996).
22. J. L. Oudar and D. S. Chemla, *J. Chem. Phys.* **66**, 2664 (1977).
23. N. H. Abramson and K. G. Spears, *Appl. Opt.* **28**, 1834 (1989).
24. S. K. Gayen and R. R. Alfano, *Opt. Photonics News* **7**, 16 (1996).
25. D. D. Steele *et al.*, *Opt. Lett.*, in press.
26. S. C. W. Hyde *et al.*, *ibid.* **20**, 1331 (1995).
27. Characterizing data: ^{1}H NMR ($CDCl_3$) δ 6.21 (s, 1H), 5.37 (s, 1H), 3.32–3.19 (m, 4H), 2.93–2.87 (m, 1H), 2.59–2.30 (m, 6H), 2.00 (m, 2H), 1.58–1.31 (m, 16H), 0.91 (t, J = 6.1 Hz, 6H). UV ($CHCl_3$) λ_{max} 496 (ε_{496} 113,500 M^{-1} cm^{-1}) nm; accurate fast atom bombardment mass spectrum (*m/z*) for M^+ $C_{25}H_{37}N_3$, calculated: 379.2987, found: 379.2979. Elemental analysis, calculated: C 79.11, H 9.82, N 11.07; found: C 78.81, H 10.01, N 10.97.
28. Supported by the U.S. Office of Naval Research (through the MURI Center CAMP), NSF, an international CNRS/NSF travel grant, the U.S. Air Force Office of Scientific Research, the U.S. Ballistic Missile Defense Organization, and a NATO travel grant. E.H. is a postdoctoral fellow of the Fund for Scientific Research–Flanders (Belgium). We thank A. Fort and M. Barzoukas from IPCMS (Strasbourg, France) for the dipole moment measurements, and P. M. Allemand for his help in the dielectric constant determination.

4 September 1997; accepted 10 November 1997

Electromechanical Properties of an Ultrathin Layer of Directionally Aligned Helical Polypeptides

T. Jaworek,* D. Neher, G. Wegner,† R. H. Wieringa, A. J. Schouten

The electromechanical properties of a monomolecular film of poly-γ-benzyl-L-glutamate (PBLG) 15 nanometers thick grafted at the carboxyl-terminal end to a flat aluminum surface were measured. The field-induced change in film thickness, dominated by a large inverse-piezoelectric effect, demonstrates that the "grafting-from" technique forces the chains into a parallel arrangement. The mechanical plate modulus of the film as determined by electrostriction agrees with the theoretical prediction for a single PBLG molecule along the chain axis. The experiments show that ultrathin polypeptide layers with large persistent polarization can be fabricated by the grafting approach.

One of the challenges of supramolecular chemistry is the manufacture of ultrathin layers with a perceptible and stable polar order. Such materials have potential in the construction of nanoscale piezo- and pyroelectric devices and for electrooptical applications. Techniques that have been used or suggested include the poling of initially nonpolar polymer films (*1*), the Langmuir-Blodgett (LB) assembly of polar monolayers (*2*), and, more recently, the defined growth of films of polar polymers by self-assembly (*3*) or grafting (*4*). In particular, the grafted films of polyglutamates have attracted interest for the fabrication of polar films (*4*–*10*). Poly-L-glutamates in the α-helical conformation are generally considered as prototype materials. The rodlike structure of the polar α-helix gives rise to some unique properties such as a high persistence length and large optical and mechanical anisotropy. In the helical conformation, the dipole moments of the individual repeat units along the chain add up to a large total dipole moment (*11*). Attempts have been made to orient polyglutamates by an electric field (*12*), and the net orientation was investigated by x-ray diffraction or second harmonic generation. However, as a consequence of the large dipole moment, the polar alignment of neighboring polypeptides helices is energetically unfavorable.

The "grafting-from" approach makes possible the directional alignment of the helical molecules (Fig. 1), as was first demonstrated by the work of Whitesell and Chang (*6*). These investigators first decorated the surface of a flat metal or metal oxide film with a layer of organic material exhibiting free amino groups by a self-assembly process and then started the polymerization of *N*-carboxyanhydrides of α-L-amino acids (NCAs) to obtain poly-L-amino acids. These amino acids are covalently attached at their COOH-terminal end to the surface and, depending on the type of amino acid used, grow directly in a helical conformation. Whitesell and Chang concluded that the chain orientation is mainly normal to the surface (*6*). However, to date, there is no conclusive evidence for proposed polar order in grafted polypeptide films.

We have measured the electromechanical properties of a grafted layer of poly-γ-benzyl-L-glutamate (PBLG) using a Nomarski optical interferometer (Fig. 2). Winkelhahn *et al.* have shown that this setup is capable of detecting periodic thickness changes with subpicometer resolution at modulation frequencies between 10 Hz and 100 kHz (*13*, *14*). The experimental data can yield the degree of polar order and the mechanical plate modulus of the ultrathin layer.

We constructed sandwich-type structures by growing a thin layer of PBLG on the surface of a glass substrate previously coated with thin aluminum strip electrodes (*15*). The self-assembled initiator layer was derived from triethoxy aminopropylsilane according to the procedure of Haller (*16*). This process generates a large surface density of amines on the substrate and prevents pinholes due to holes in the initiator layer (*17*). The surface graft polymerization initiated by the surface-anchored amino groups was carried out at 40°C in a 0.5 M solution of *N*-carboxyanhydride monomer in *N*,*N*-dimethylformamide for 2 days under nitrogen atmosphere. Further experimental details on the polymerization will be published elsewhere (*18*). The thickness of the grafted layer was 15 nm, as determined with a Tencor α-step profiler (*19*). The top aluminum strip electrodes were deposited with an orientation perpendicular to that of the bottom strips. In this way six independent

T. Jaworek, D. Neher, G. Wegner, Max-Planck-Institut für Polymerforschung, Ackermannweg 10, 55128 Mainz, Germany.
R. H. Wieringa and A. J. Schouten, Department of Polymer Chemistry, University of Groningen, Nijenborgh 4, 9747 AG Groningen, Netherlands.

*Present address: Tokyo Institute of Technology, Research Laboratory of Resources Utilization, 4259 Nagatsuta, Midori-ku, Yokohama, 226 Japan.
†To whom correspondence should be addressed. E-mail: wegner@mpip-mainz.mpg.de

Infrared Photorefractive Polymers and Their Applications for Imaging

B. Kippelen *et al.*

Science **279**, 54 (1998);
DOI: 10.1126/science.279.5347.54